Unveiling the Underlying Influence of pH on the Crystallization of Hybrid Perovskite Materials, Delivering Low Voltage Loss Photovoltaics

Nakita K. Noel,[1] Martina Congiu,[1,2] Alexandra J. Ramadan,[1] Sarah Fearn,[3] David P. McMeekin,[1] Jay B. Patel,[1] Michael B. Johnston,[1] Bernard Wenger,[1*] Henry J. Snaith.[1*]

[1] Clarendon Laboratory, Department of Physics, University of Oxford, Parks Road, Oxford, OX1 3PU, United Kingdom

[2] Centre for Nanoscience and Technology, Italian Institute of Technology, via Giovanni Pascoli 70/3, Milano 20133, Italy

[3] Department of Materials, Imperial College London, London, SW7 2AZ, United Kingdom.

[*] Corresponding authors: henry.snaith@physics.ox.ac.uk, bernard.wenger@physics.ox.ac.uk

Supporting Information

Materials and Methods:

Synthesis of Methylammonium Iodide: Methylammonium iodide (MAI) was synthesised according to previously published methods.[1] Briefly, methylamine (33 wt.% in ethanol, Sigma Aldrich) was added to HI (57 wt.% in H_2O, Sigma Aldrich) in ethanol with stirring, under inert conditions. The mixture was left stirring for 4 hours at room temperature. The MAI was crystallised by driving off the ethanol using a rotary evaporator. The MAI was recrystallized from warm ethanol and washed using

diethyl ether, followed by vacuum drying. After drying the MAI was kept in a desiccator until use.

Dimethylamine Bubbling: A 38 wt.% precursor solution of $CH_3NH_3PbI_{3-x}Cl_x$ was prepared by dissolving MAI and $PbCl_2$ in DMF at a 3:1 molar ratio. After the powders were dissolved, dimethylamine was bubbled into the solution using previously reported methodology. [2] Bubbling was done for for 1, 3, 5 or 7 minutes as required.

Fabrication of Planar Heterojunction Solar Cells: Planar heterojunction solar cells were fabricated utilising previously published methods.[3, 4] Concisely, FTO-coated glass sheets ($7\Omega cm^{-1}$ Hartford Glass) were etched with zinc powder and HCl (3M) to obtain the required electrode pattern. The sheets were then washed with soap (2% Hellmanex in water), deionized water, acetone, ethanol and isopropanol, and finally treated under oxygen plasma for 10 min to remove the last traces of organic residues. A compact layer of SnO_2 was then deposited on the glass using a modified version of the methodology presented by Anaraki et al.[5] Briefly, $SnCl_4.5H_2O$ was dissolved in isopropanol at a concentration of 0.05M and stirred at room temperature for 1 hour. The solution was then spincoated onto the substrates at 3000 rpm, after which the substrates were annealed at 180˚C for 1 hour before being left to naturally cool down to room temperature. The substrates were then immersed into a chemical bath , which consisted of $SnCl_2 \cdot 2H_2O$ (Sigma-Aldrich) in deionised water (0.012 M), 20.7 mM urea (Sigma-Aldrich), 0.15 M HCl (Fisher scientific) and 2.87 μM 3-mercaptopropionic acid (Sigma-Aldrich). The substrates were kept in an oven at 70 °C for 180 min, after which they were sonicated in deionised water for 2 minutes. They were then washed with ethanol and annealed at 180 °C for 60 min. The required amount of formic acid or dimethylamine

was added to the 38 wt.% perovskite precursor solution in DMF such that the overall concentration of the solution was kept constant (3:1 molar ratio of MAI: $PbCl_2$) ($PbCl_2$, Sigma Aldrich 98 %). The precursor solution was then spin coated directly onto the substrate at 2000 rpm in a nitrogen filled glove box. The substrate was then left to dry under N_2 for 10 min before being placed on a hotplate at 90°C where it was annealed for 180 min. For the mixed-cation, mixed halide perovskite, a 1.25M solution of $FA_{0.83}MA_{0.17}Pb(I_{0.83}Br_{0.17})_3$ was prepared using a 4:1 vol.:vol. ratio of DMF:DMSO. The solution was spincoated onto the desired substrate at 1000 rpm for 10 s, followed by 6000 rpm for 35 s. 100 µL of anisole was dropped onto the substrate 35 s after the beginning of the spincoating. The films were then annealed at 100 °C for 60 min. After annealing, the substrate was allowed to cool down to room. Subsequently, the hole transport material (HTM) was dissolved in chlorobenzene (85 mg/mL with 30 mol % Li-TFSI and 80 mol % tBP as additives), and was spin coated onto the perovskite substrates at 2000 rpm. 100 nm thick silver electrodes were then deposited under high vacuum (10^{-6}) through a shadow mask.

UV-Vis Spectrophotometry: The steady-state absorption spectra were acquired with a Perkin-Elmer Lambda 1050 UV/Vis/NIR spectrophotometer. A stock solution of thymol blue was prepared by dissolving 1 mg/mL of thymol blue (Sigma Aldrich) in dimethyl sulfoxide (DMSO). The thymol blue solution was then added to neat and acidified anhydrous dimethylformamide (DMF) such that the concentration of indicator in the final solution was 10 vol.%. Measurements were taken in a temperature controlled cuvette holder with constant stirring. All steady state absorption spectra were acquired at 25 ˚C. For temperature dependent measurements, the solution was held at 25 ˚C for 2 minutes, after which the solution was gradually

heated (over 15 minutes) to 95 ˚C, where it was held for 5 minutes, before being cooled back down to room temperature.

Transmission and absorption spectra of thin films were collected using a Varian Cary 300 UV-Vis spectrophotometer with an integrating sphere.

Dynamic Light Scattering (DLS): The DLS experiments were performed with a Zetasizer Nano ZS instrument (Malvern Instruments, UK), equipped with a 633 nm He-Ne laser. In a typical experiment each sample is measured three times with 15 runs per measurement (10-15 seconds per run). The temperature was stabilised during 120 seconds prior to the acquisition of the data. All samples were measured in the backscattering mode. Most samples showed high polydispersity, therefore the autocorrelation decays are fitted with a multimodal distribution model.

Secondary Ion Mass Spectroscopy:

Secondary ion mass spectrometry (SIMS) analyses were performed on an IONTOF ToF-SIMS V instrument. The primary ion beam was a 25keV Bi^+ in BAM (bunched to 4 pulses to avoid detector saturation). The sputter beam was Cs+ at 1keV and a beam current of 75nA. The analytical area was 100um^2 with a sputter crater of 300um^2.

Current-Voltage Characterisation: Solar cell performance was measured using a class AAB ABET sun 2000 solar simulator that was calibrated to give simulated AM 1.5 sunlight at an irradiance of 100 mW/cm^2 . The irradiance was calibrated using an NRELcalibrated KG5-filtered silicon reference cell. Currentvoltage curves were recorded using a sourcemeter (Keithley 2400, USA). All solar cells were masked with a metal aperture that was used to

define the active area of the devices, which in this case was 0.0925 cm^2. All devices were stored in a desiccator in the dark for 12 h prior to testing.

External Quantum Efficiency Measurements: External quantum efficiency (EQE) was measured via custom build Fourier transform photocurrent spectrometer based on a Bruker Vertex 80v Fourier Transform Interferometer. Devices were illuminated with an AM1.5 filtered solar simulator. Devices were calibrated to a Newport-calibrated reference silicon solar cell with known external quantum efficiency. The devices were masked with a metal aperture with a defined active area, 0.0919 cm^2.

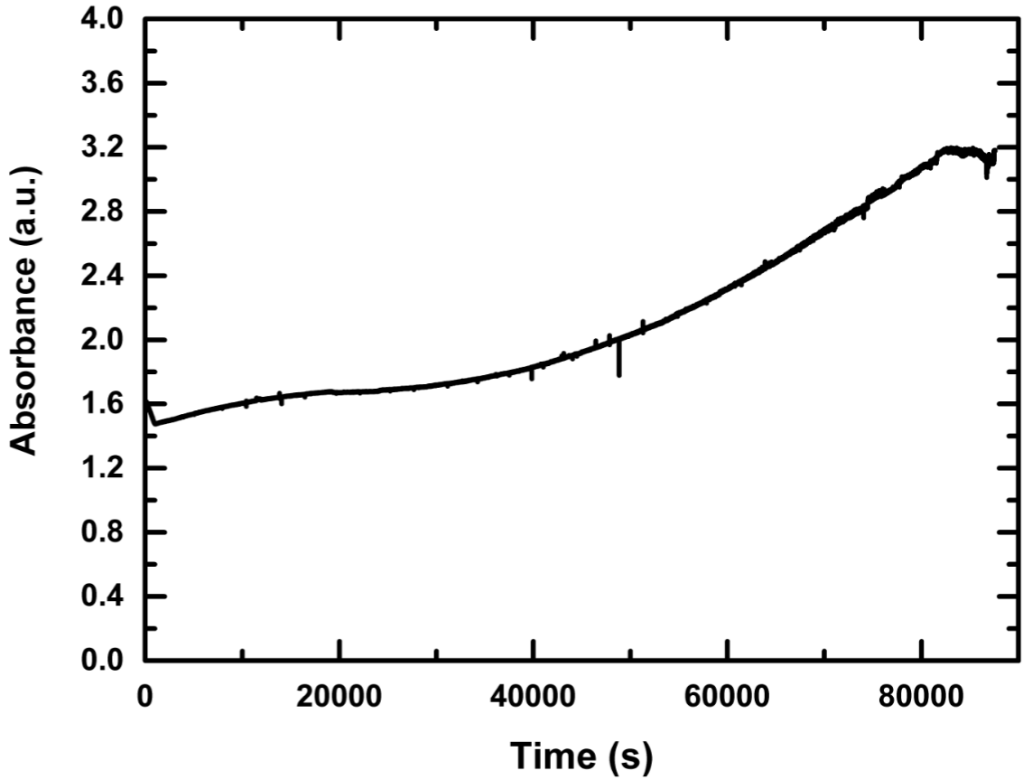

Figure S1: Absorbance of thymol blue in DMF at 402 nm when solution is held at 95 °C and measured continuously for 24 hrs.

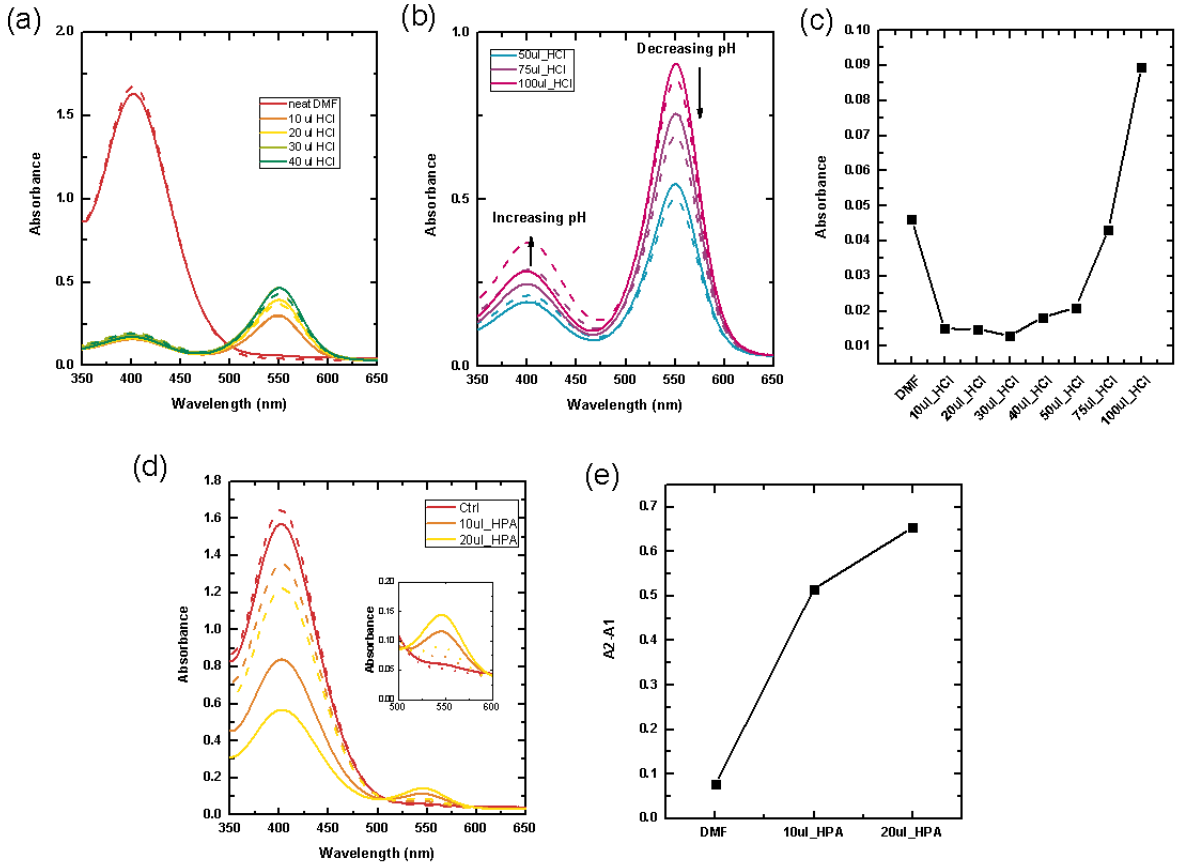

Figure S2: (a), (b) and (d) Absorption spectra of thymol blue in neat, and acidified DMF before (solid lines) and after (dashed lines) temperature cycling. (c) and (e) Difference in the peak 402 nm absorbance before and after temperature cycling.

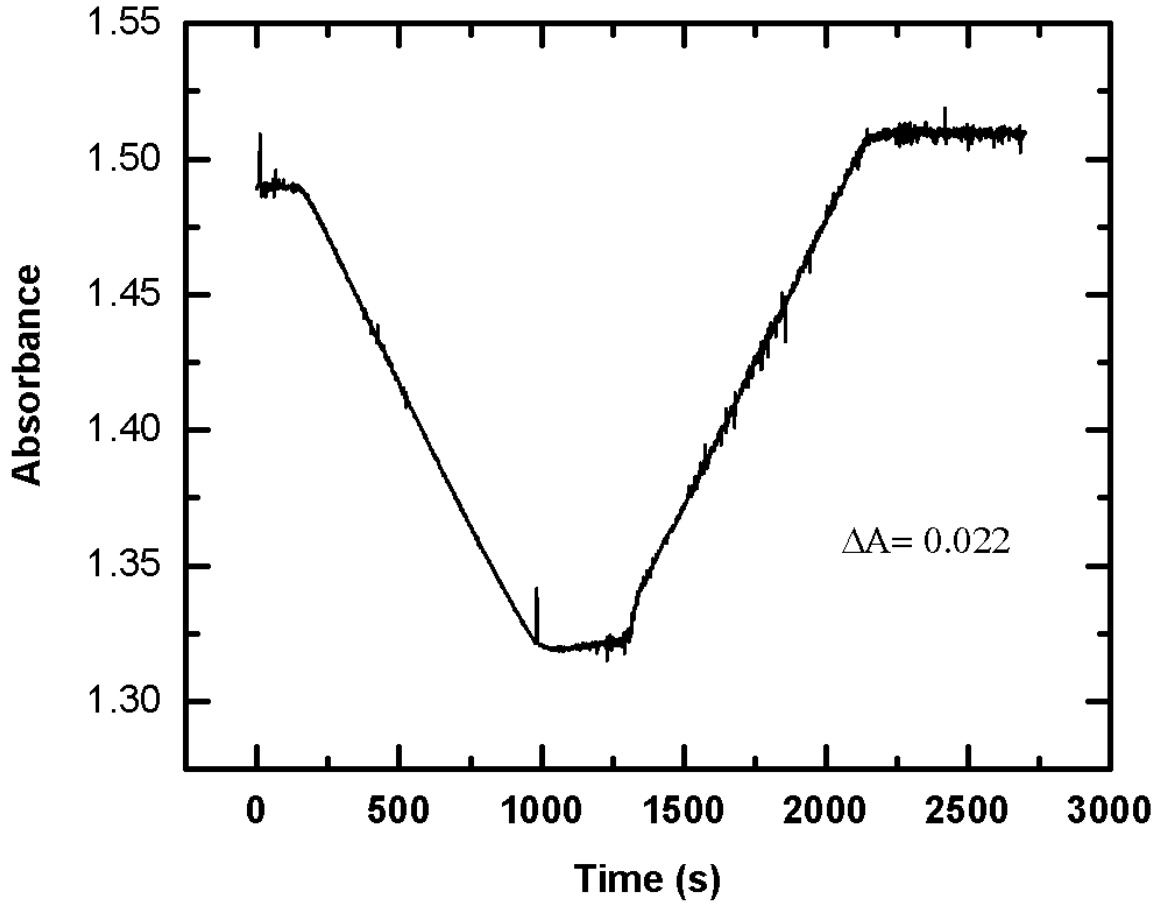

Figure S3: Evolution in the absorbance of thymol blue in DMF + 100 µL/mL of H_2O at 402 nm, with time and temperature.

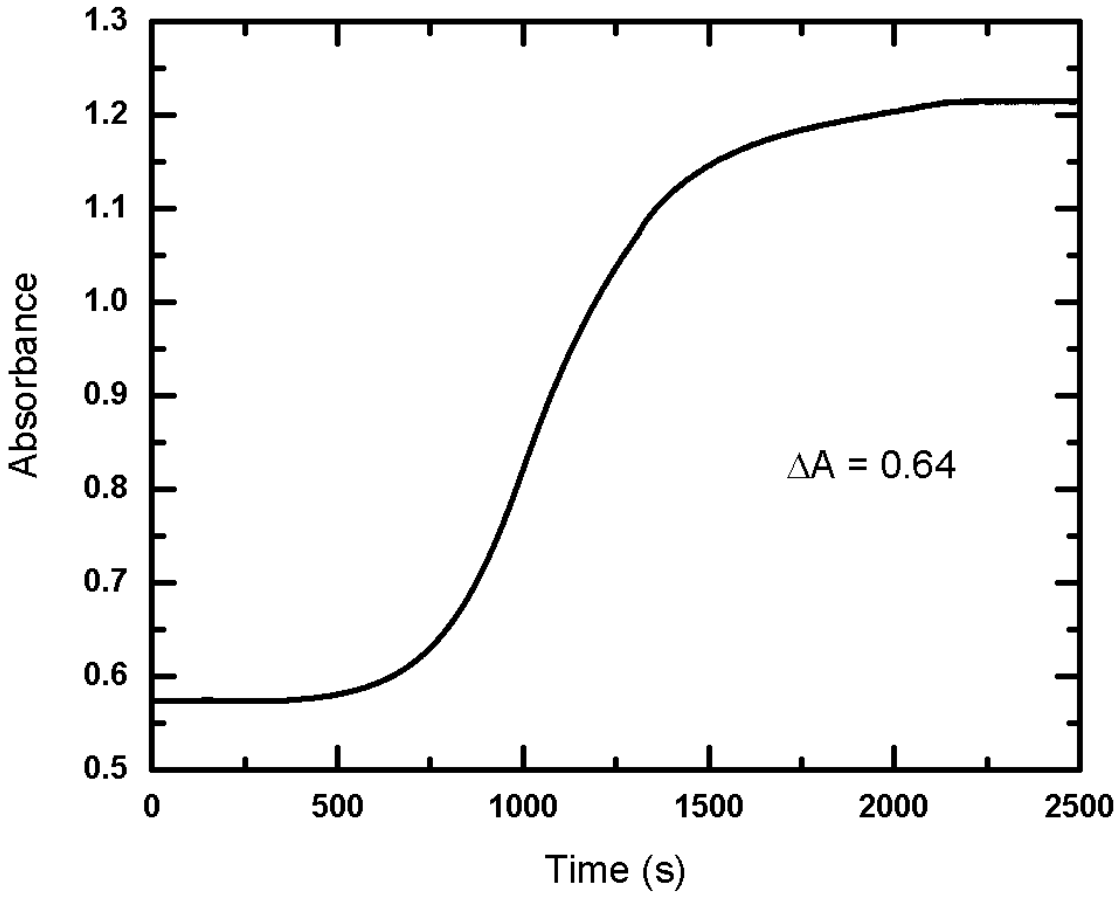

Figure S4: Evolution in the absorbance of thymol blue in DMF with 20 µL of HPA at 402 nm, with time and temperature.

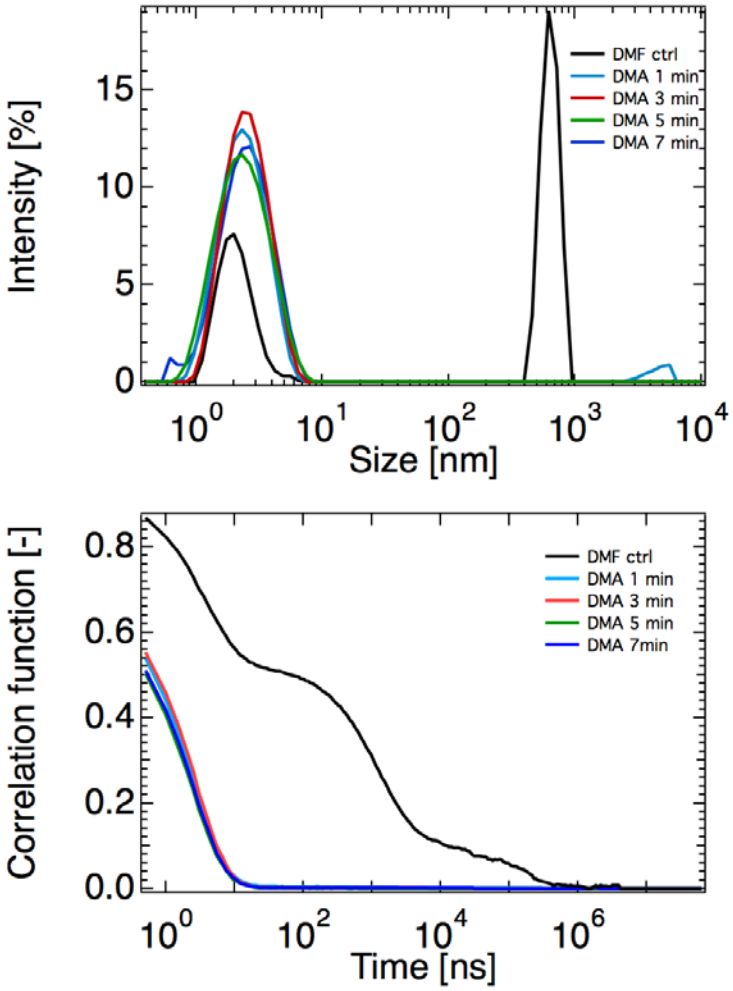

Figure S5: Dynamic Light Scattering. Change in the colloid size and distribution of $CH_3NH_3PbI_{3-x}Cl_x$ with the addition of dimethylamine, bubbled into the solution for 0, 1, 3, 5 and 7 minutes.

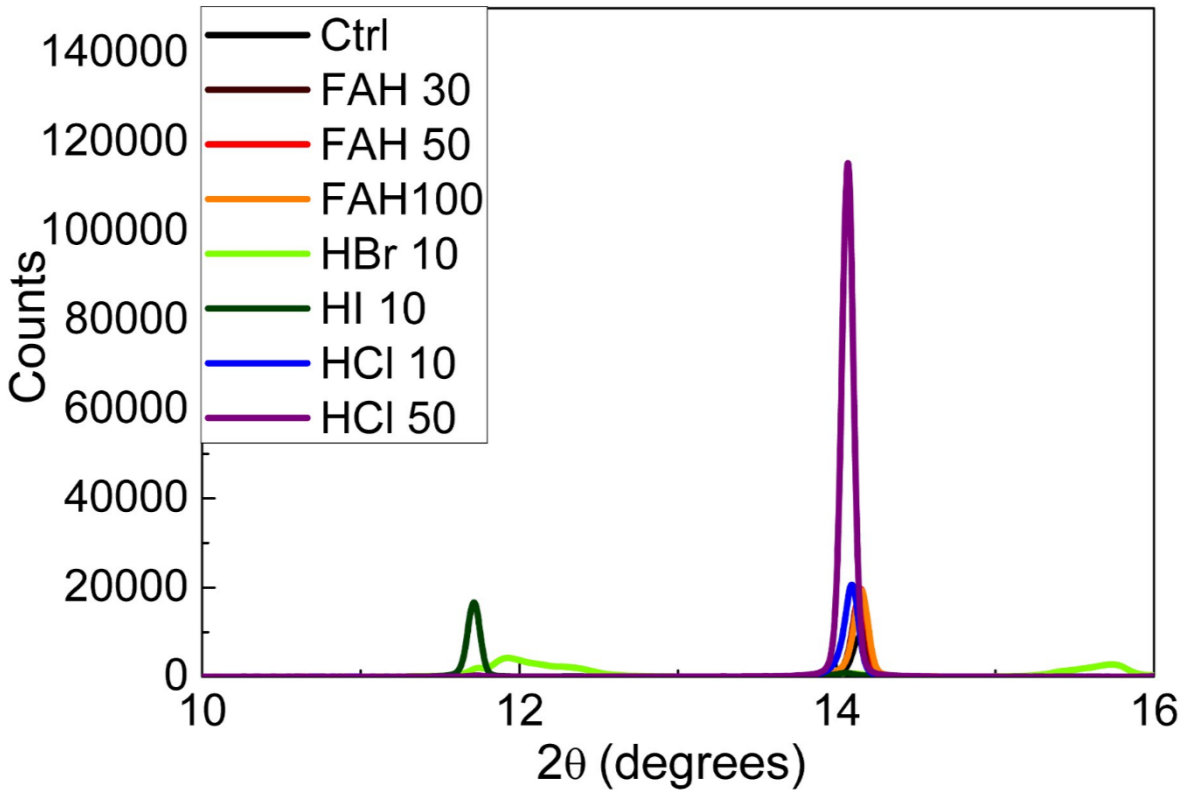

Figure S6: X-Ray Diffraction. X-ray diffraction patterns of $CH_3NH_3PbI_3$ films fabricated from neat DMF (ctrl), and DMF acidified with varying amounts of formic acid (FAH) and hydrohalic acids.

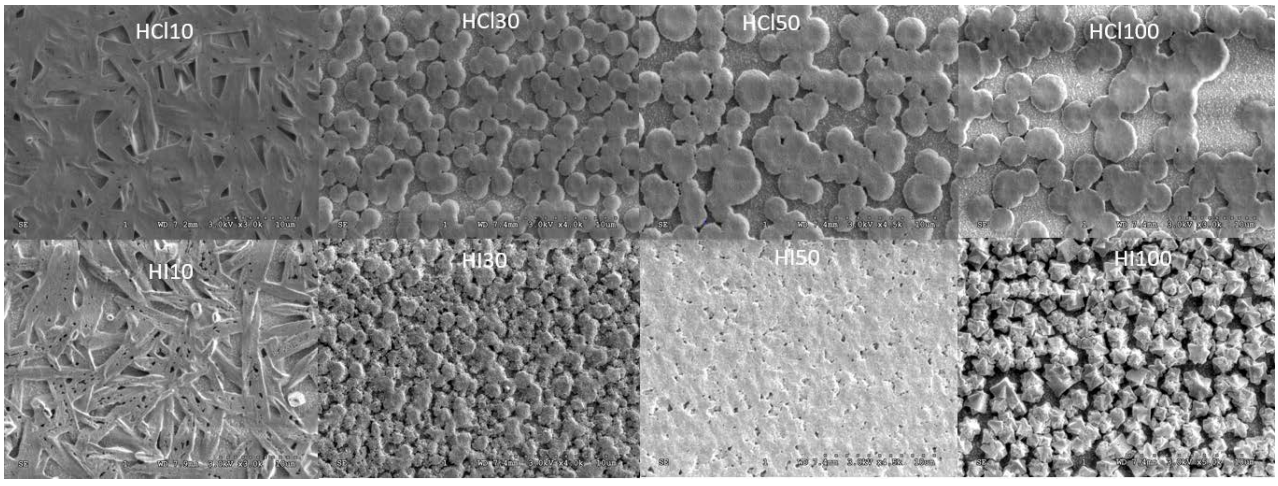

Figure S7: Scanning Electron Microscopy. SEM images of $CH_3NH_3PbI_{3-x}Cl_x$ films fabricated with various amounts of HI and HCl added to the precursor solution.

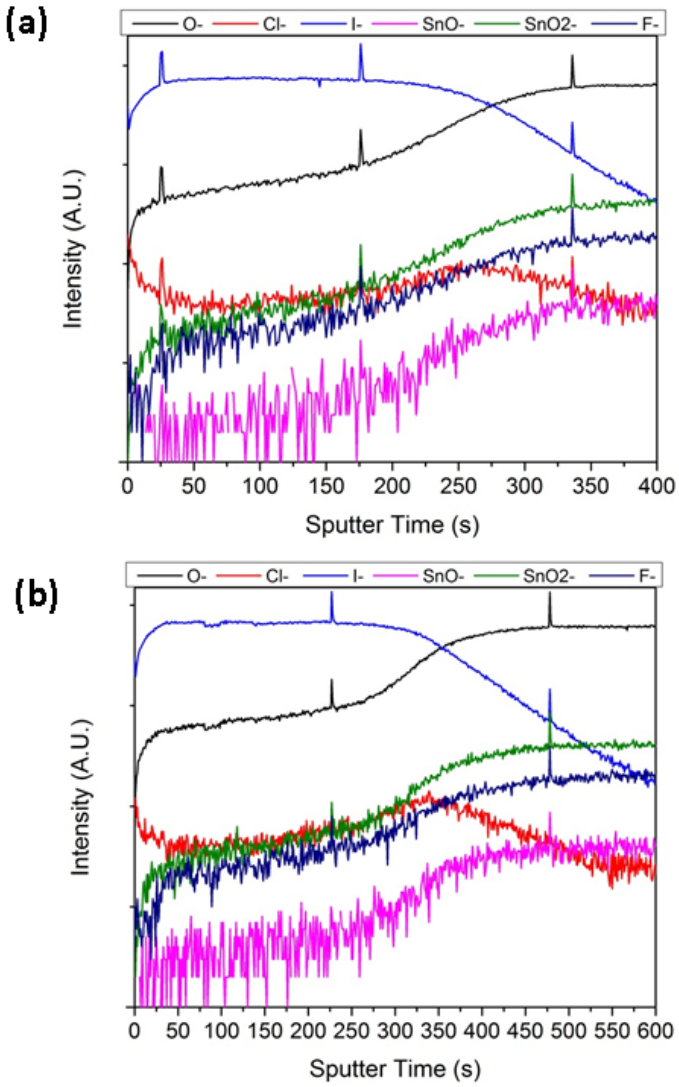

Figure S8: Secondary Ion Mass Spectroscopy. Spectrographs of films of $CH_3NH_3PbI_{3-x}Cl_x$ films fabricated from precursor solutions with (a) neat DMF, and (b) DMF and 30 µL/mL of formic acid.

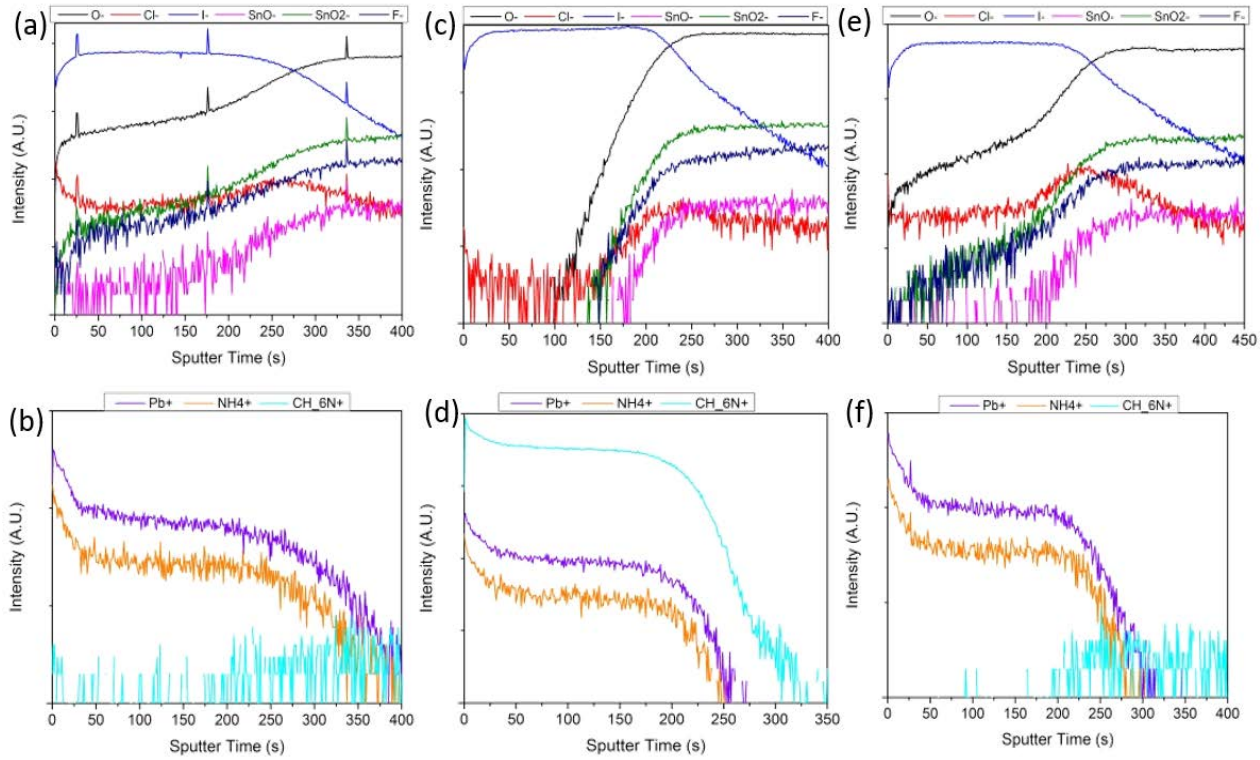

Figure S9: Secondary Ion Mass Spectroscopy. Spectrographs of films of $CH_3NH_3PbI_{3-x}Cl_x$ films fabricated from precursor solutions with neat DMF (a)and (b), and 0.02 vol.% of HCl (c) and (d), and HI (e) and (f).

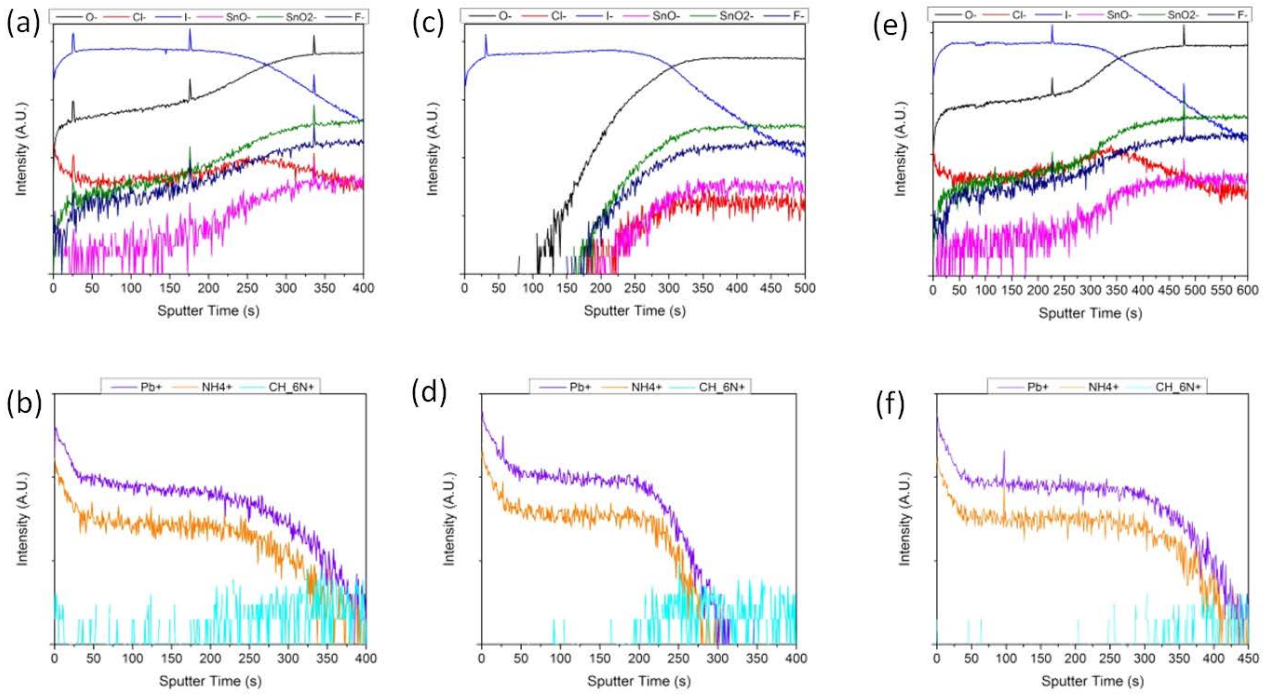

Figure S10: Secondary Ion Mass Spectroscopy. Spectrographs of films of $CH_3NH_3PbI_{3-x}Cl_x$ films fabricated from precursor solutions with neat DMF (a)and (b), and 0.02 vol.% of HPA (c) and (d), and formic acid (e) and (f).

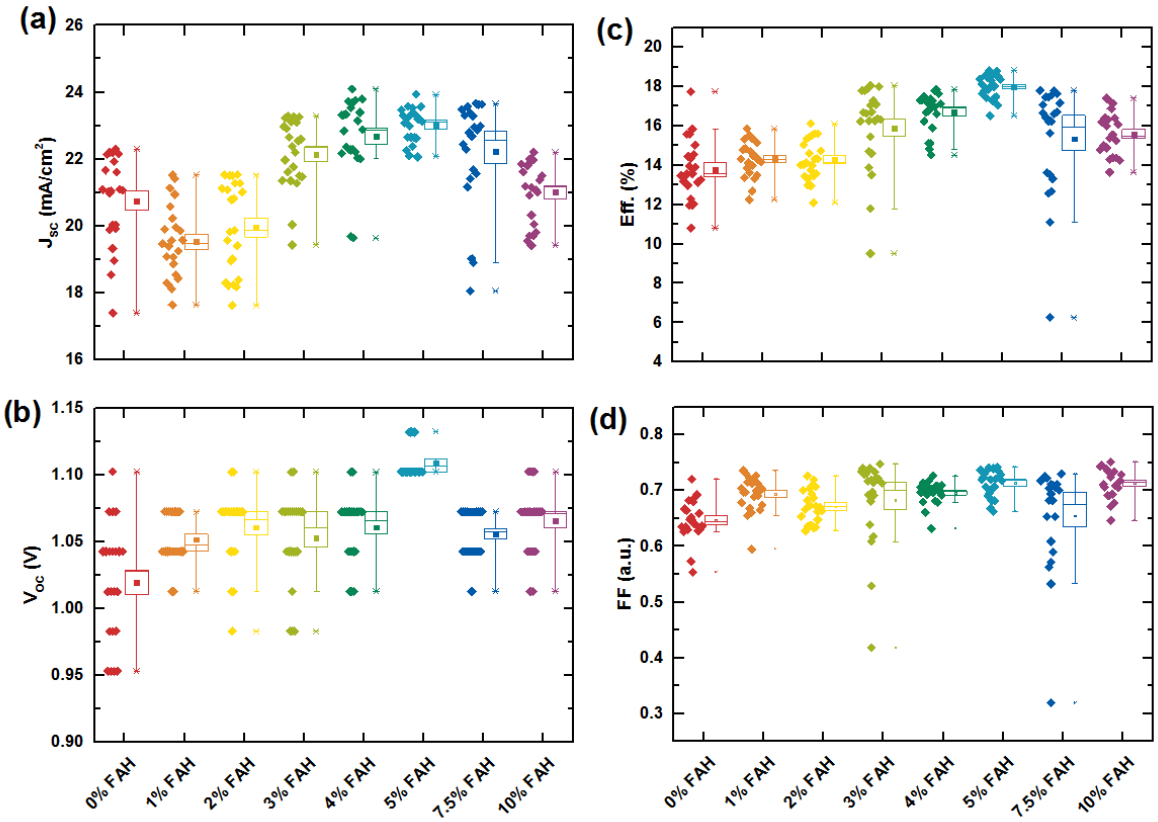

Figure S11: Statistics on the performance parameters of solar cells fabricated from neat and acidified DMF-based $CH_3NH_3PbI_{3-x}Cl_x$ precursor solutions.

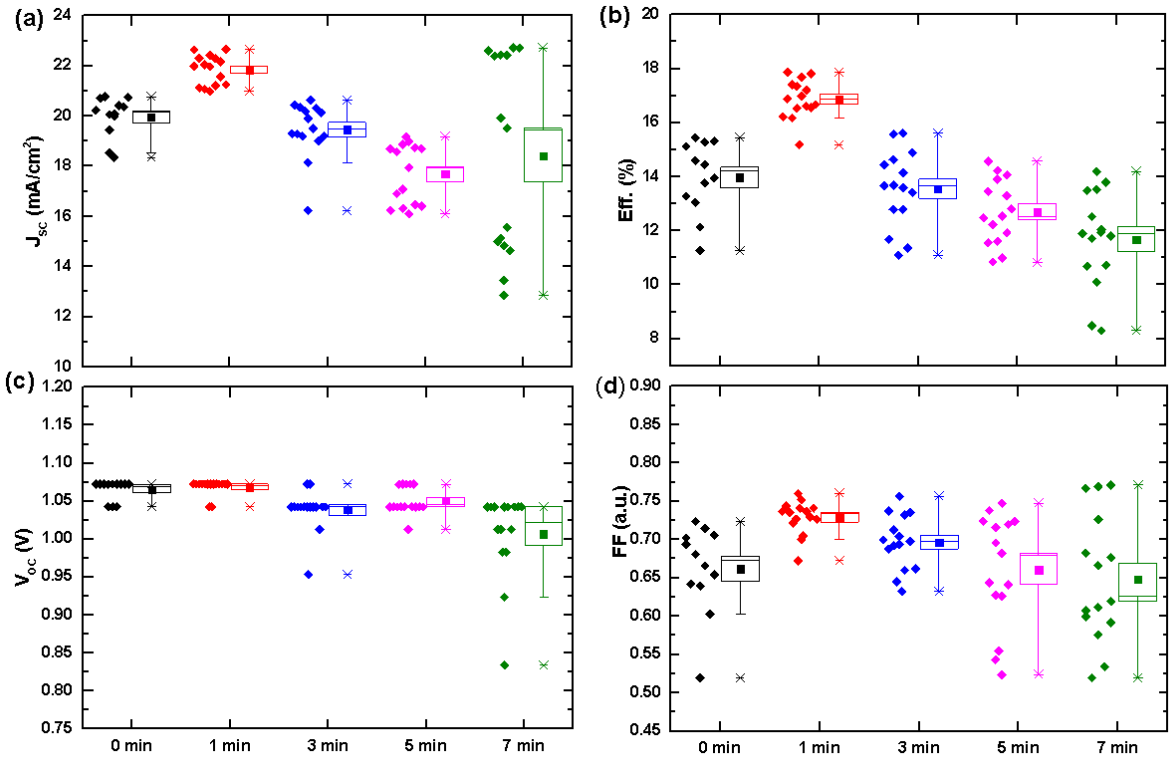

Figure S12: Statistics on the performance parameters of solar cells fabricated from neat and alkalinized DMF-based $CH_3NH_3PbI_{3-x}Cl_x$ precursor solutions. Solutions were bubbled with dimethylamine for 1 min, 3 min, 5 min and 7 min.

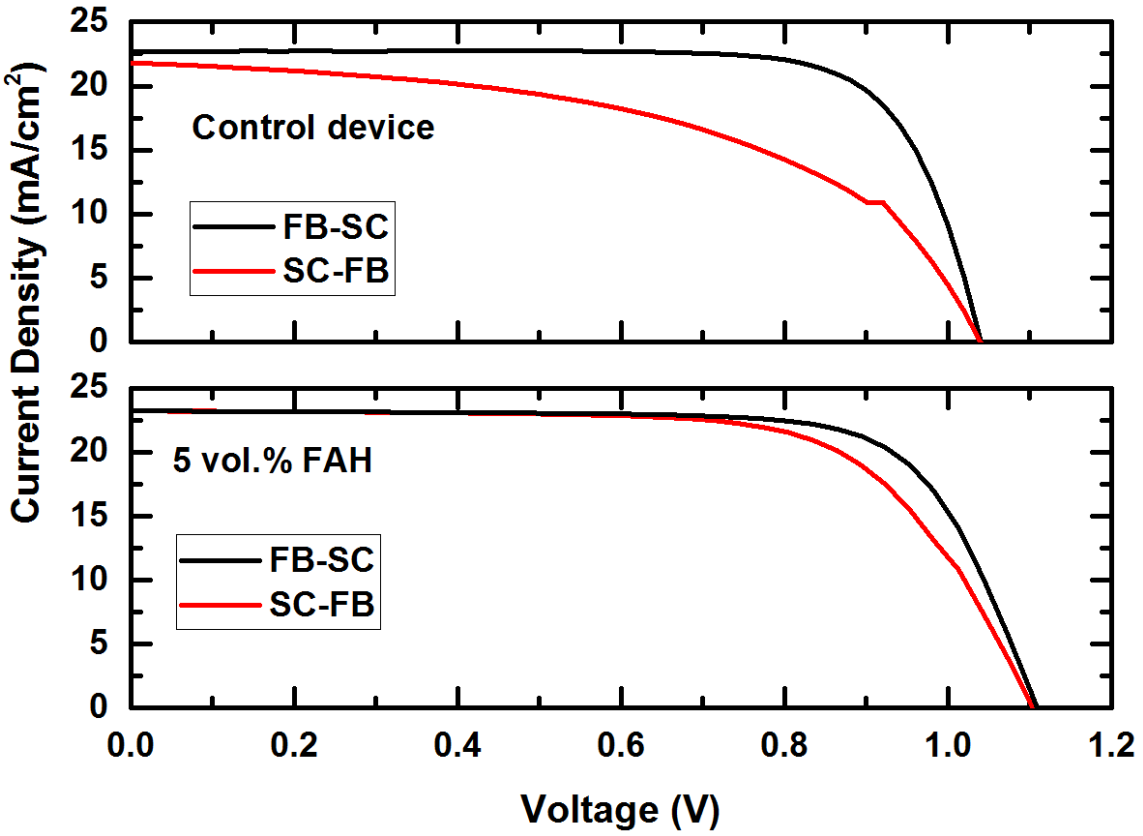

Figure S13: Current-Voltage curves of the solar cells fabricated from a neat, and an acidified precursor solution of $CH_3NH_3PbI_{3-x}Cl_x$.

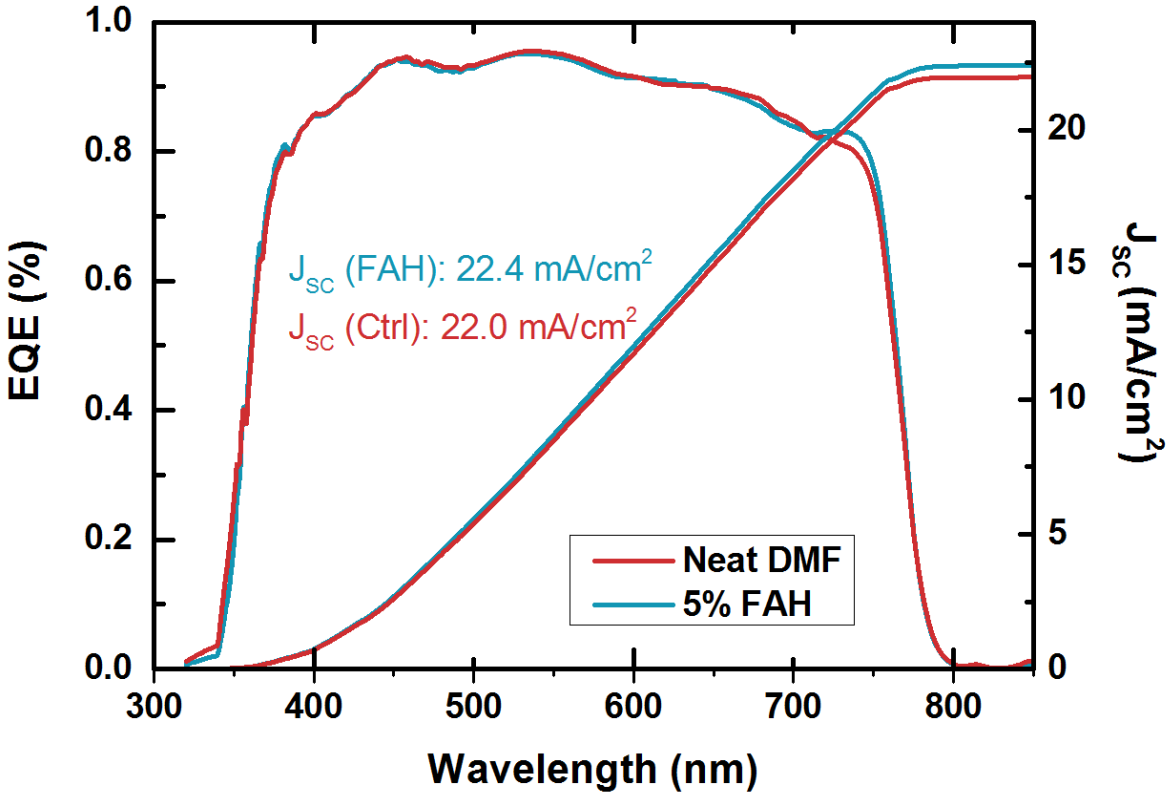

Figure S14: External Quantum Efficiency of champion $CH_3NH_3PbI_{3-x}Cl_x$ devices fabricated from neat DMF and from DMF with formic acid, giving integrated current densities of 22.0 mA/cm^2 and 22.4 mA/cm^2 respectively. Both values are in good agreement with the J_{SC} obtained during the current-voltage characterisations.

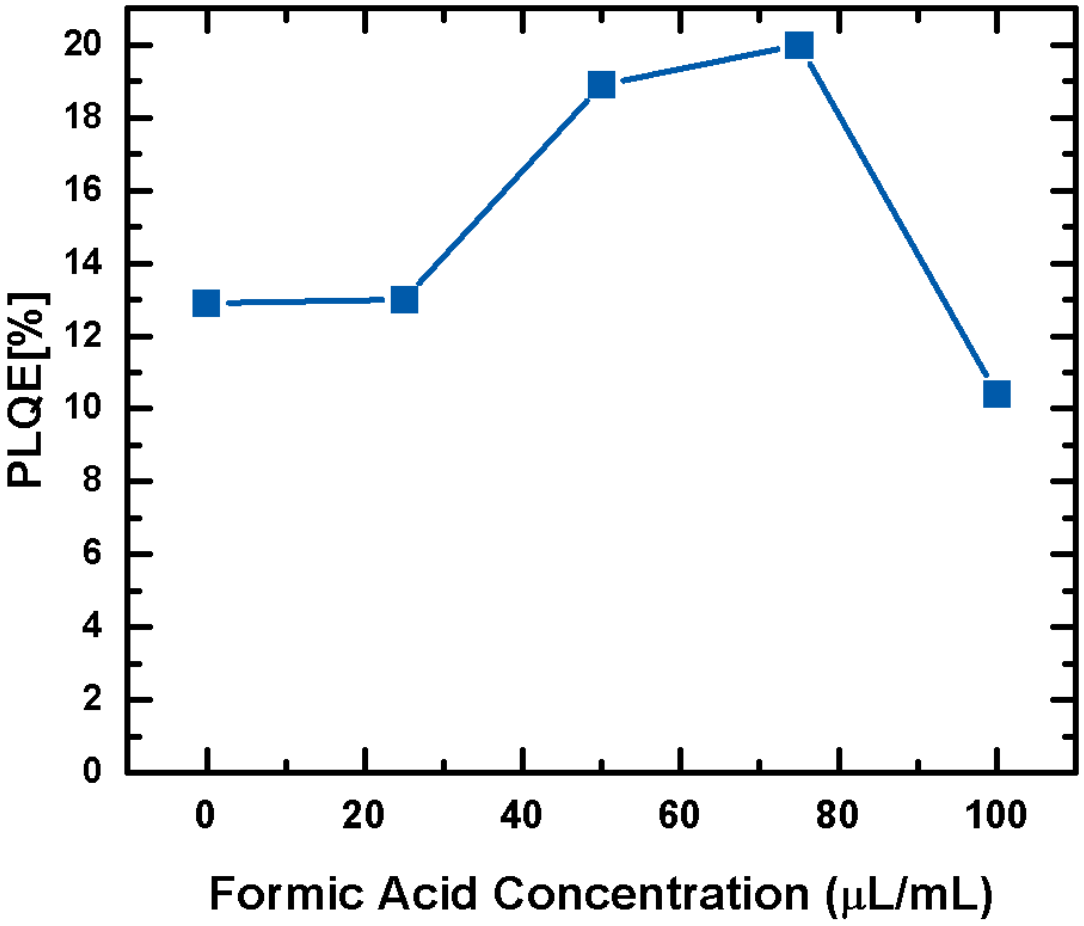

Figure S15: Photoluminescence quantum efficiencies of $FA_{0.83}MA_{0.17}Pb(I_{0.83}Br_{0.17})_3$ films fabricated from precursor solutions with varying concentrations of formic acid.

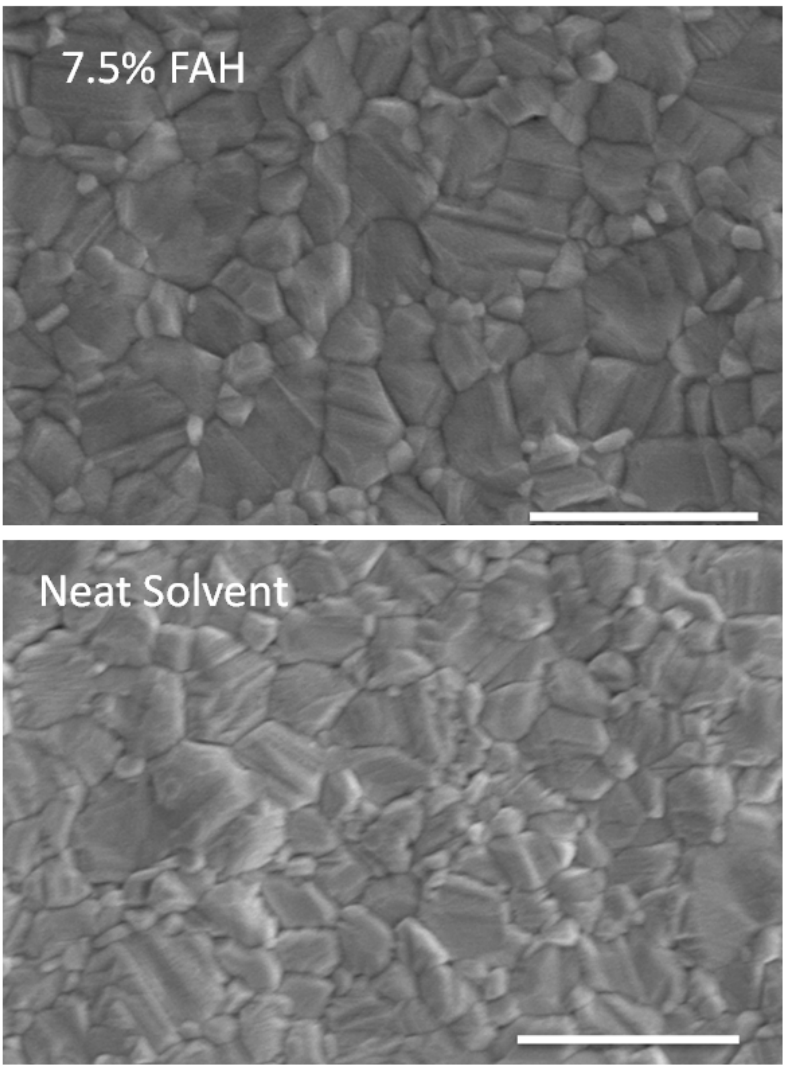

Figure S16: SEM images of $FA_{0.83}MA_{0.17}Pb(I_{0.83}Br_{0.17})_3$ films fabricated from precursor solutions with and without formic acid.

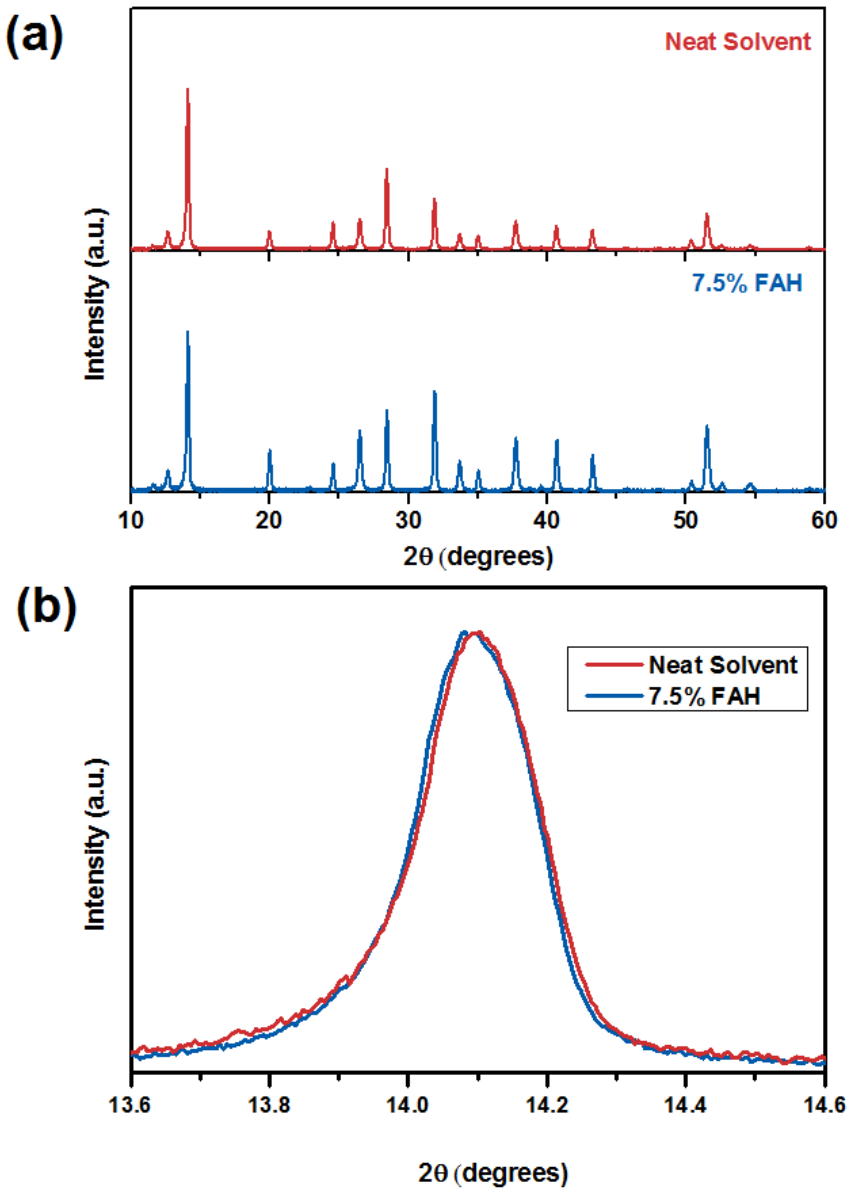

Figure S17: (a) X-Ray diffraction patterns of films of $FA_{0.83}MA_{0.17}Pb(I_{0.83}Br_{0.17})_3$ films fabricated from precursor solutions made with neat solvent, and solvent with 7.5 vol.% formic acid. (b) Close-up view of the 110 peak of the perovskite films fabricated with and without acid, showing almost identical peak widths and intensities. The difference in the ratio of the intensities of the peaks shown in the films fabricated with and without formic acid, indicates a slight difference in the orientation of the crystals in the film.

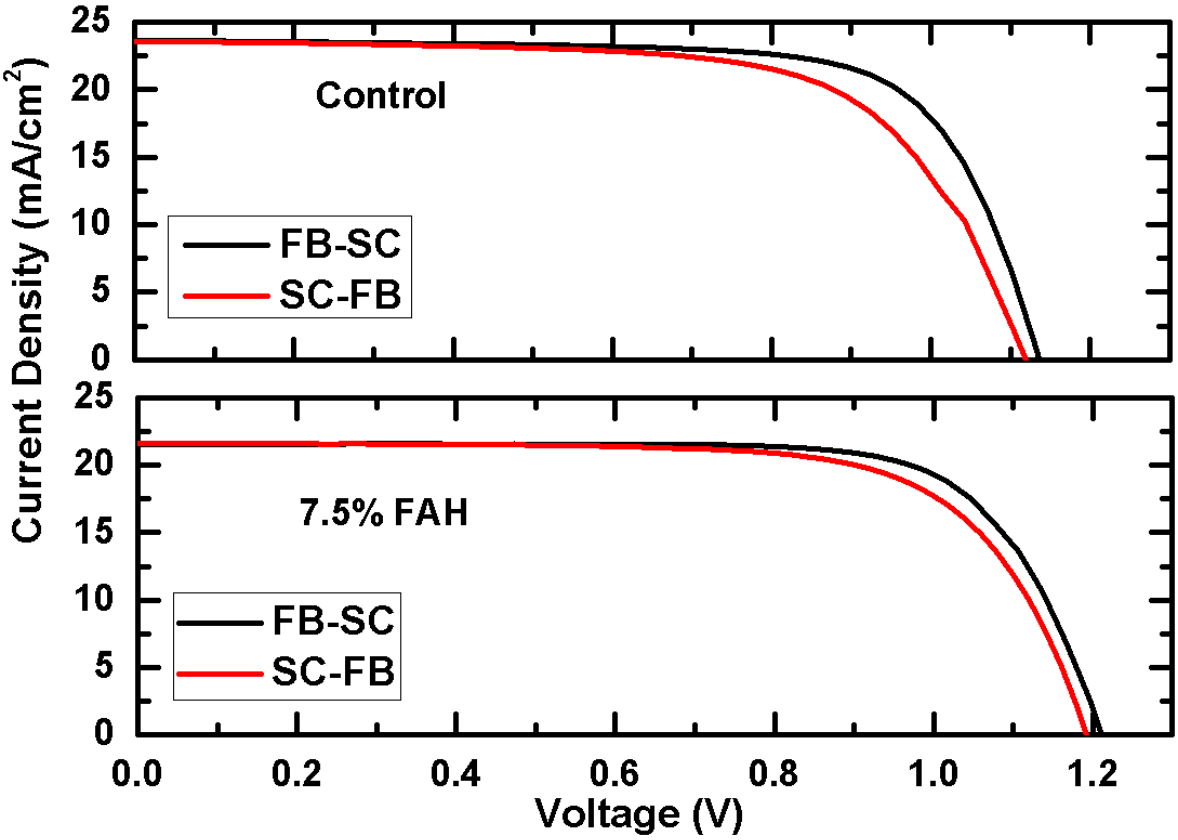

Figure S18: Forward and reverse current-Voltage curves of the solar cells fabricated from a neat, and an acidified precursor solution of the mixed-cation, mixed-halide perovskite $FA_{0.83}MA_{0.17}Pb(I_{0.83}Br_{0.17})_3$.

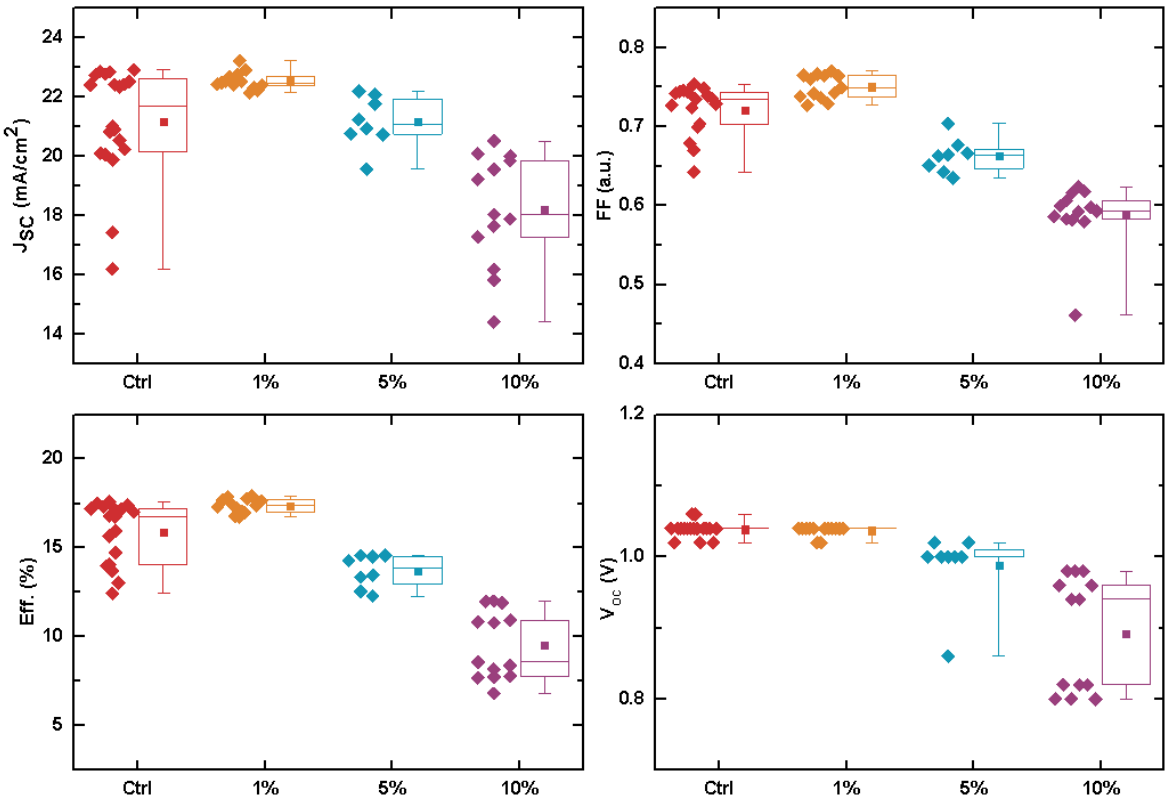

Figure S19: Performance parameters for a batch of $CH_3NH_3PbI_{3-x}Cl_x$ devices where the compact layer was pre-treated with acidified DMF at different concentrations of FAH.

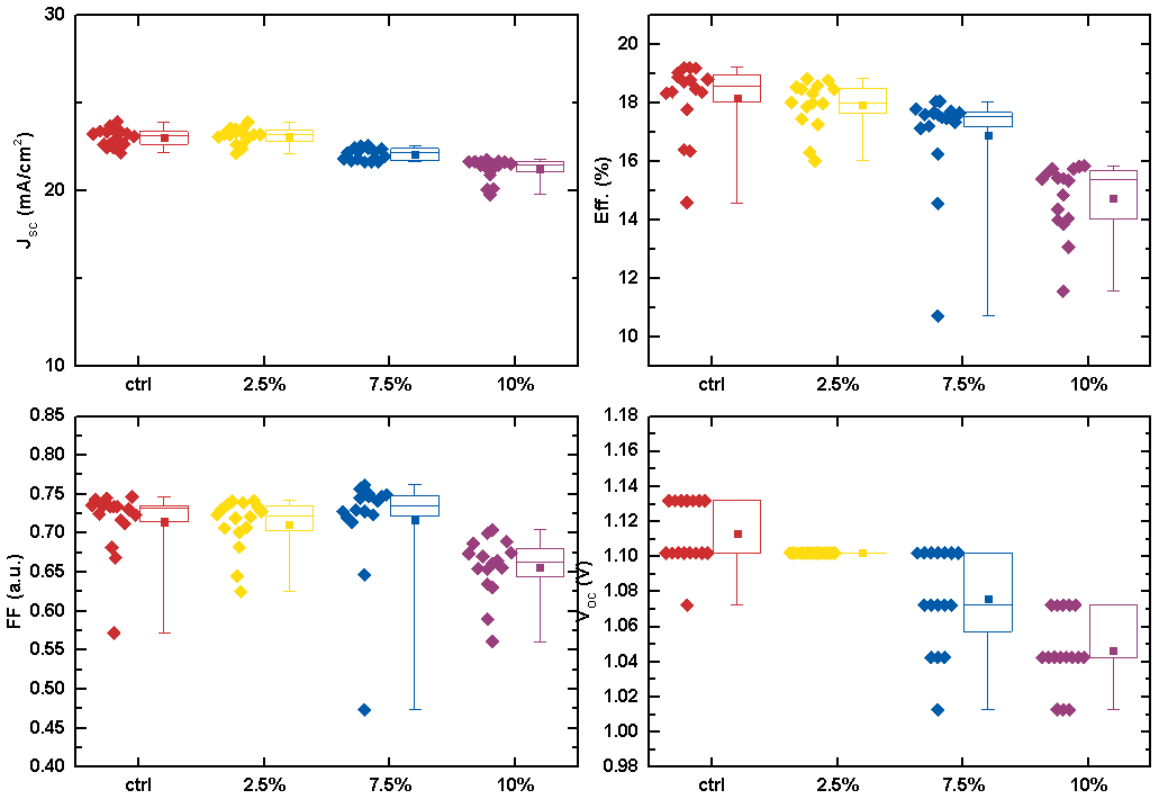

Figure S20: Performance parameters for a batch of $FA_{0.83}MA_{0.17}Pb(I_{0.83}Br_{0.17})_3$ devices where the compact layer was pre-treated with acidified DMF at different concentrations of FAH.

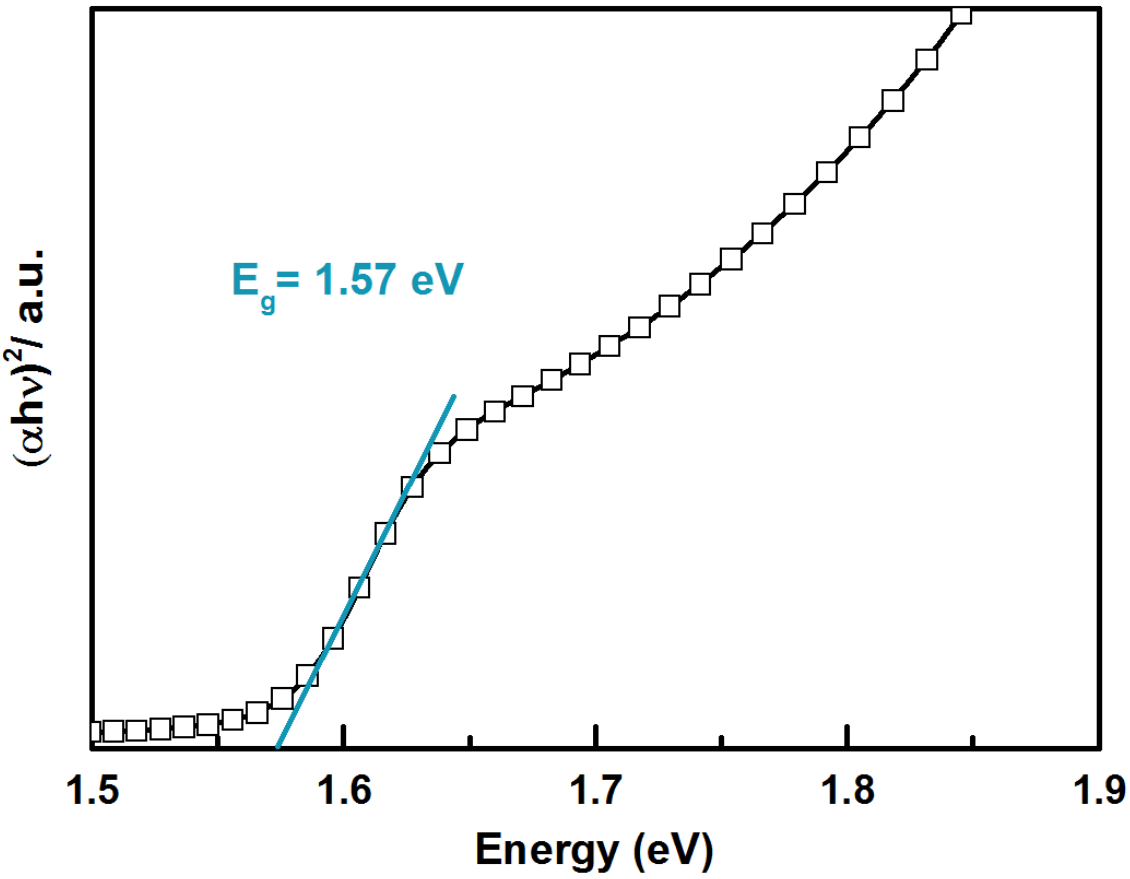

Figure S21: Tauc plot showing the band gap determination of the mixed-cation, mixed-halide perovskite $FA_{0.83}MA_{0.17}Pb(I_{0.83}Br_{0.17})_3$, assuming a direct band gap material.

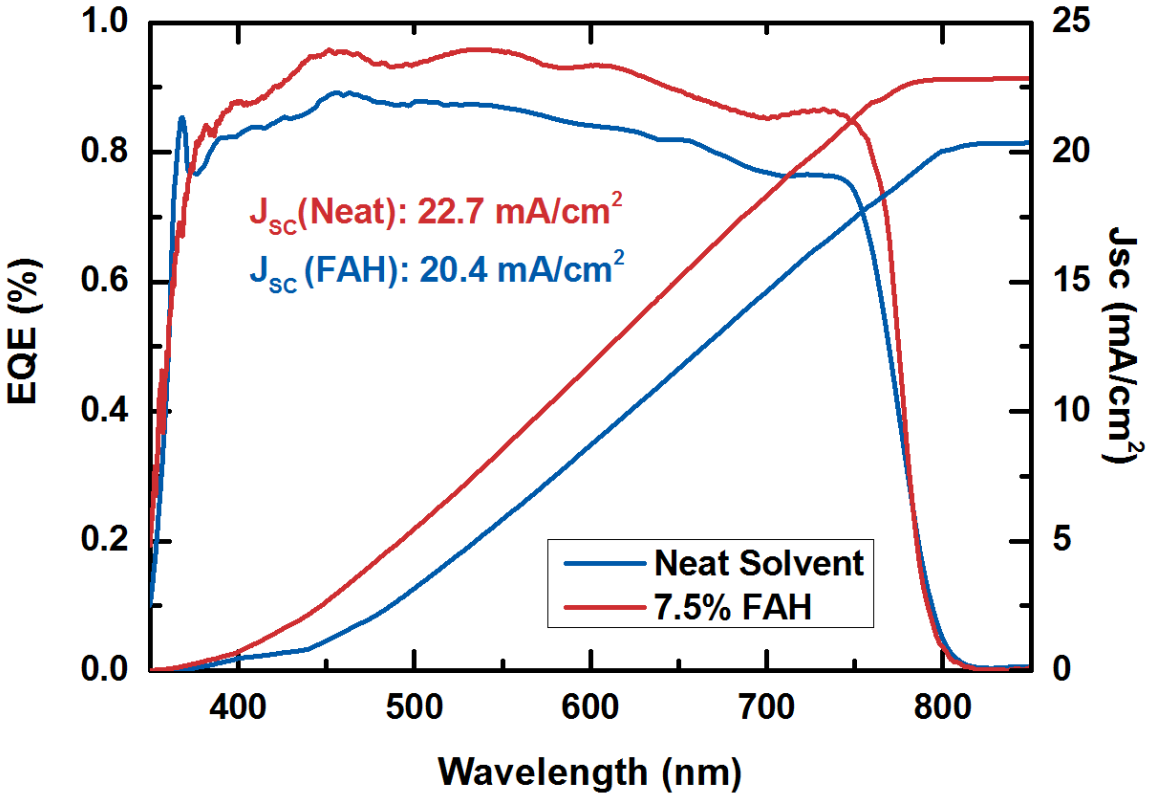

Figure S22: External Quantum Efficiency of champion $FA_{0.83}MA_{0.17}Pb(I_{0.83}Br_{0.17})_3$ device fabricated with and without formic acid, giving integrated current densities of 20.4 mA/cm^2 and 22.7 mA/cm^2 respectively.

References:

1. M. M. Lee, J. Teuscher, T. Miyasaka, T. N. Murakami and H. J. Snaith, *Science*, 2012, **338**, 643-647.
2. N. K. Noel, S. N. Habisreutinger, B. Wenger, M. T. Klug, M. T. Horantner, M. B. Johnston, R. J. Nicholas, D. T. Moore and H. J. Snaith, *Energy & Environmental Science*, 2017, **10**, 145-152.
3. G. E. Eperon, V. M. Burlakov, P. Docampo, A. Goriely and H. J. Snaith, *Advanced Functional Materials*, 2013, DOI: 10.1002/adfm.201302090, n/a-n/a.
4. N. K. Noel, A. Abate, S. D. Stranks, E. S. Parrott, V. M. Burlakov, A. Goriely and H. J. Snaith, *ACS Nano*, 2014, **8**, 9815-9821.

5. E. H. Anaraki, A. Kermanpur, L. Steier, K. Domanski, T. Matsui, W. Tress, M. Saliba, A. Abate, M. Gratzel, A. Hagfeldt and J.-P. Correa-Baena, *Energy & Environmental Science*, 2016, **9**, 3128-3134.